Critical sets in discrete Morse theories: relating Forman and piecewise-linear approaches

THOMAS LEWINER

Department of Mathematics — Pontifícia Universidade Católica — Rio de Janeiro — Brazil

Abstract. Morse theory inspired several robust and well grounded tools in discrete function analysis, geometric modeling and visualization. Such techniques need to adapt the original differential concepts of Morse theory in a discrete setting, generally using either piecewise–linear (PL) approximations or Forman's combinatorial formulation. The former carries the intuition behind Morse critical sets, while the latter avoids numerical integrations. Forman's gradients can be constructed from a scalar function using greedy strategies, although the relation with its PL gradient is not straightforward. This work relates the critical sets of both approaches. It proves that the greedy construction on two-dimensional meshes actually builds an adjacent critical cell for each PL critical vertex. Moreover, the constructed gradient is globally aligned with the PL gradient. Those results allow adapting the many works in PL Morse theory for triangulated surfaces to Forman's combinatorial setting with low algorithmic complexity.

Keywords: ***Morse theory. Forman theory. Piecewise linear approximation. PL topology. Critical set. Morse–Smale decomposition. Reeb graphs. Computational topology.***

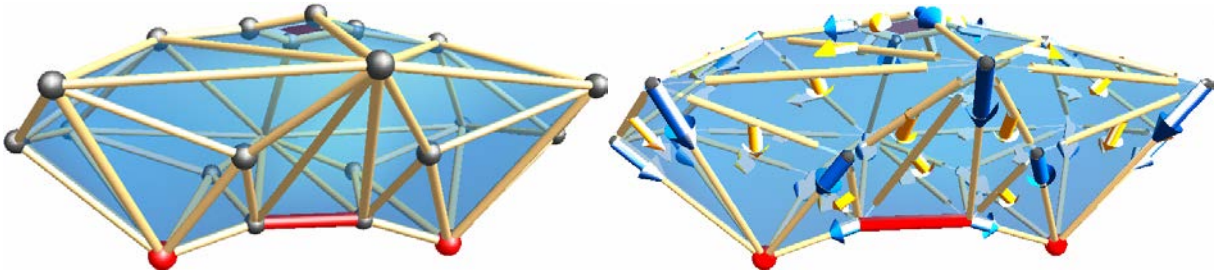

Figure 1: *Critical cells obtained from the greedy construction (there is a critical face at the top), with f being the vertical projection (left). The direction of the gradient is also coherent (right).*

1 Introduction

Topological methods provide robust and well-grounded techniques to analyze and process discrete geometric models [33]. Among those, Morse theory defines a very direct framework to study scalar functions or gradient vector fields on manifolds. Morse proved that the number and nature of critical points of regular gradient fields is constrained by the manifold on which it is defined [29]. Smale further extended those results to coherently decompose the manifold in cells of trivial dynamic under the gradient field [40]. In practice, this theory allows to check the coherence of mesh data structures [10, 27] and scalar functions analysis [41] such as physical quantities in numerical simulation [8], and grounds effective methods to visualize their main features [12, 3].

Morse's theory were originally defined for differentiable manifolds, and thus computer-aided applications rely on approximations or discrete versions of their concepts. The most straightforward approximation of a scalar function on a mesh is given by piecewise-linear (PL) functions. Banchoff [2] proposes a definition of critical points in that setting, which has been extended to several applications, in particular for visualization [3] and reconstruction [20, 45, 39]. The approximation approach has the advantage of carrying most of the intuition of the smooth setting.

Forman [15] developed a combinatorial formulation that completely extends Morse results to general cell complexes. This approach fits directly into the polygonal mesh setting, which is common in modeling and graphics. However, Forman's definitions are rather combinatoric than geometric (Figure 1), which complicates the construction of a discrete vector field $\mathcal{V}$ directly from a smooth function f. In particular, a cell in Forman's theory should contain points of similar dynamics under the vector field, and its dimension must represent the nature of the critical element. For example, the minima of f must be located at vertices, which in extreme cases may turn the positioning of critical cells non-intuitive (Figure 2).

Preprint MAT. 02/11, communicated on February 3^{rd}, 2010 to the Department of Mathematics, Pontifícia Universidade Católica — Rio de Janeiro, Brazil. The corresponding work was published in Computer Aided Geometric Design, Elsevier, 2012..

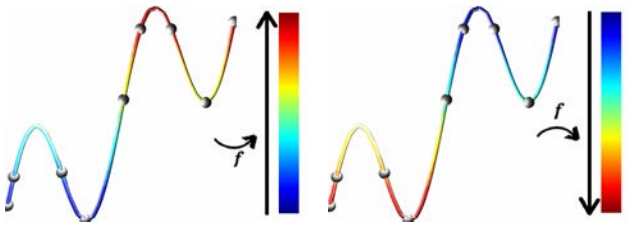

Figure 2: *A discrete curve with a scalar function f defined as the vertical projection. Forman's restriction on the dimension of critical cells may lead to non–intuitive position of critical cells. (left) The complex is well adapted to f: minima are located at vertices and almost all the maxima on edges. (right) The complex is not adapted to f: the smooth minima occur out of the vertices, and critical vertices cannot coincide with them.*

Contributions In this paper, we study the properties of greedy constructions of Forman's discrete gradient vector field from scalar functions defined on the mesh vertices [25, 5] as compared to PL approximations. We prove that, under regularity restrictions, Forman's critical cells defined by the greedy construction are adjacent to Banchoff's PL critical vertices (Figure 1). We further prove that the discrete gradient globally follows the directions of $-\nabla f$. Those results open several computer applications of Morse theory currently based on PL approximations to Forman's approach, which would improve on simplicity and numerical stability while keeping performance. In particular, we mention the discrete Morse–Smale decomposition, persistence computation and Reeb graph construction.

Related work Banchoff's definition of PL critical points [2, 38] brought Morse theory to several applications, among which the effective construction of contour trees [4, 34], persistence [11, 6] and visualization [14]. There have been many works on PL Morse–Smale decomposition [12, 13] with improvements for visualization [3, 30].

Regarding Forman's approach, early works propose to construct discrete Morse functions with as few critical cells as possible: using lexicographic orderings [1], greedy strategies for undirected spanning trees [23, 25] and integer programming [19]. Then, real applications pushed for the construction of discrete Morse function representing a sampled scalar function, using greedy strategies on directed spanning trees [25, 5, 26] of local cancellations or successive, non-local cancellations in particular for volumetric data [17, 18]. More recently, weighted graph matching approaches cleverly approximate vector fields in multi–resolution [35, 36, 37].

The present work uses a greedy strategy similar to [22, 25] but on undirected spanning trees, which is already used in several applications [5, 43, 44]. To our knowledge, no guarantee on the critical cells position has been presented yet. This work represents part of the author's PhD thesis [26].

Notation For cell complexes, we follow Forman's notation [15]: A cell complex K is a coherent collection of cells. We focus on surfaces, so the dimension p of cell σ^p is 0, 1 and 2 for vertices, edges and faces respectively. The incidence relation is denoted by $\sigma^p \succ \tau^{p-1}$. The scalar function f is defined on the set of vertices K_0, with real values. We consider here K as a triangulated manifold without boundary, although Forman's results apply to more general complexes.

2 Basics of Morse Theories

Morse theory relates the topology of a manifold $\mathcal{M}$ and the dynamics of gradient vector fields $\mathcal{V}$ defined on $\mathcal{M}$. Basically, the topology of $\mathcal{M}$ constrains the number and nature of critical elements of the gradient, and conversely those elements may help characterizing the topology of $\mathcal{M}$. In this section, we briefly recall the original formulation on smooth manifolds together with Banchoff's definition for piecewise-linear functions on triangulated manifolds [2] and with Forman's combinatorial matchings on general cell complexes [15]. Although all those theories are valid in any dimension, we focus here on two–dimensional manifolds to state our main results.

(a) Smooth Morse Theory

Given a smooth surface $\mathcal{M}$, classical Morse theory studies smooth scalar functions $f : \mathcal{M} \to \mathbb{R}$ and the dynamics of their gradient vector fields $-\nabla f$. The *critical set* of f is the set of surface points where the gradient vanishes: $\nabla f(\mathbf{x}) = 0$. From the gradient dynamics, critical points are the end points of the integral lines of $-\nabla f$. A function f is valid if its critical set is discrete, i.e. critical points are isolated. In that case, the Hessian matrix of f is non-singular at the critical points.

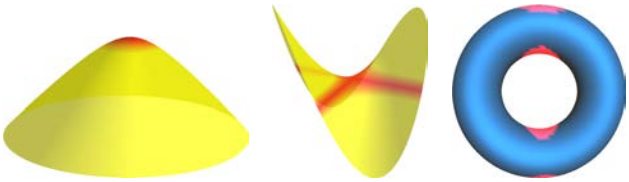

Figure 3: *Critical points for the vertical projection, marked as the middle of the red region: (left) maximum (minimum for -f) and (middle) saddle. The standard torus has one minimum, two saddles and a maximum: $\#_0 - \#_1 + \#_2 = 1 - 2 + 1 = 0 = \chi(\mathcal{M})$.*

The Morse lemma [28] classifies critical points according to the local dynamic of $-\nabla f$. More precisely, since the Hessian matrix at a critical point $\mathbf{x}$ is non-singular, it has p negative eigenvalues and $2 - p$ positive ones, and the integer p is called the *index* q $(\mathbf{x})$ of $\mathbf{x}$. Then, f near one of its critical points $\mathbf{x}$ is locally similar to the quadratic form deduced from its Hessian matrix. The index thus characterizes the critical point: an index 0 means $\mathbf{x}$ is a local minimum, an index 2 that $\mathbf{x}$ is a local maximum. Critical points of index 1 are saddle points (Figure 3).

The corresponding work was published in Computer Aided Geometric Design, Elsevier, 2012..

Figure 4: *Two combinatorial fields on a 1–dimensional complex: the left one has a close $\mathcal{V}$–path and is not a gradient. The right one is valid, with its critical set (2 vertices, 2 edges) in red.*

From this lemma, Morse deduced that all the level sets $f^{-1}(t)$ for $t \in [a,b]$ have the same homotopy type iff they do not contain any critical point [28]. Moreover, the change of level set topology at a critical value a is completely characterized by the index of critical points $\mathbf{x}$ with $f(\mathbf{x}) = a$. This result leads to the Morse inequalities relating the number $\#_p$ of critical points of index p with the topology of $\mathcal{M}$. In particular, $\#_0 - \#_1 + \#_2 = \chi(\mathcal{M})$, the Euler characteristic of $\mathcal{M}$.

(b) Piecewise-Linear Morse Theory

Banchoff extended Morse inequalities to functions f defined on polyhedrons K (without boundary) by piecewise linear (PL) interpolation from scalar values $f(\tau)$ at vertices τ [2]. In order to preserve the behavior characterized by Morse lemma, Banchoff defines critical points as a break in the monotony of f. More precisely, a PL function is valid if its values $f(\tau)$ at vertices are pairwise distinct. The *lower star* of vertex τ is the set of edges and faces for which τ is the vertex with maximal value through f. The *Banchoff index* $\mathrm{idx}(\tau)$ of τ is the Euler characteristic of its lower star.

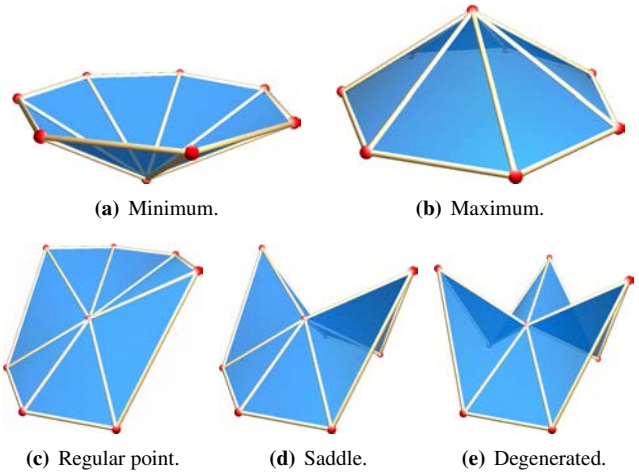

(a) Minimum. **(b)** Maximum. **(c)** Regular point. **(d)** Saddle. **(e)** Degenerated.

Figure 5: *Banchoff's classification of generic points on surfaces, and a non–generic saddle (e), where the values of f on the vertices is its height (z coordinate).*

For a local minimum, the lower star is reduced to vertex τ, and the Banchoff index is thus $\mathrm{idx}(\tau) = 1$ (Figure 5). For a local maximum, the lower star is an open disk (all the faces and edges incident to τ, with τ itself), which leads to Banchoff index $\mathrm{idx}(\tau) = 1$. For a regular point, the lower star is a semi-open disk, which gives a Banchoff index of $\mathrm{idx}(\tau) = 0$. Finally, a regular saddle is a wedge sum on τ of two semi-open disks, leading to index $\mathrm{idx}(\tau) = -1$.

Observe that this definition differs from the Morse index $q(\tau)$. However, for non–degenerated critical vertices, $\mathrm{idx}(\tau) = (-1)^{q(\tau)}$. Banchoff index relates to the Euler characteristic by $\chi(K) = \sum_{\tau \in K_0} \mathrm{idx}(\tau)$. This definition of critical points is also related with end points of integral lines obtained by numerical integration on triangular meshes, which is the starting point for PL Smale decomposition [12].

(c) Forman's Discrete Morse Theory

Instead of functions, Forman grounds his interpretation on vector fields, whose local direction is described as vertex/edge and edge/face matchings [15]. More precisely, a *combinatorial vector field* $\mathcal{V}$ is a collection $\left\{\left(\tau^p \prec \sigma^{p+1}\right)\right\}$ of disjoint pairs of incident cells. We represent a matching $\left(\tau^p \prec \sigma^{p+1}\right)$ by an arrow from τ^p to σ^{p+1} (Figure 4). The disjointness condition means that a cell is either the source or the destination of at most one arrow.

The equivalent of the *integral line* is called a *$\mathcal{V}$–path*. It is a sequence of cells $\blacktriangleleft \tau_0^p\ \sigma_0^{p+1}\ \tau_1^p\ \sigma_1^{p+1}\ \ldots \sigma_{k-1}^{p+1}\ \tau_k^p \blacktriangleright$ where τ_i and τ_{i+1} are distinct faces of σ_i and $(\tau_i, \sigma_i) \in \mathcal{V}$. Observe that a $\mathcal{V}$–path contains cells of only two dimensions.

If a cell σ^p does not belong to any pair, it can only be an endpoint of a $\mathcal{V}$–path, and similarly to the smooth case, it is said to be *critical*. The index of the critical cell is its dimension p, and coincides exactly with the Morse index q.

A $\mathcal{V}$–path is *closed* when the last cell equals the first cell: $\tau_k^p = \tau_0^p$ (Figure 4). A valid *discrete gradient vector field* is a combinatorial vector field with no closed $\mathcal{V}$–path. All the Morse inequalities are valid with that definition. However, the construction of a combinatorial field from a function sampled on the vertices is delicate.

3 Position of PL and Forman Critical Sets

We consider here a greedy approach [25, 5, 26] to build a discrete vector field $\mathcal{V}$, in Forman's definition, from a scalar function sampled on the vertices $f : K_0 \to \mathbb{R}$, as in Banchoff's PL setting. This approach successively adds *directed* pairs $\left(\tau^p \prec \sigma^{p+1}\right)$ of adjacent cells to $\mathcal{V}$ if neither τ^p nor σ^{p+1} is already matched and if this addition does not close a $\mathcal{V}$–path. The scalar function f is used to sort the pairs to be added through a weight function: $\mathsf{W}_f((\tau \prec \sigma)) = \bar{f}(\sigma) - \bar{f}(\tau)$, where $\bar{f}$ is defined on a cell σ as the mean of the values of f on the vertices of σ. The pairs with lower weight are considered first.

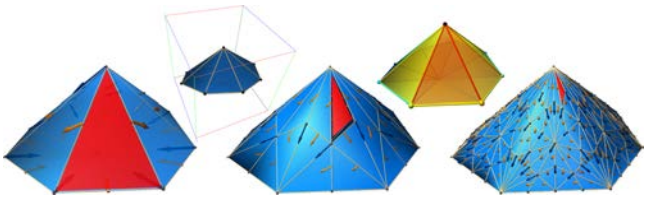

Figure 6: *Successive barycentric subdivisions preserve the PL maximum (top vertex), while the greedy construction builds a discrete Morse function with a critical cell adjacent to it. In this example, the scalar function f corresponds to the coordinate of the green axis (top row).*

Although this procedure is efficient[1], it is not clear *a priori* that it is able to capture the features of f. In this section, we prove that the $\mathcal{V}$–paths generated by the algorithm are decreasing, i.e. aligned with $-\nabla f$. We further demonstrate that, for surfaces under some regularity assumptions, the algorithm builds a critical cell adjacent to each vertex that is critical under the PL definition.

More precisely, after one barycentric subdivision, PL minima coincide with critical vertices of the greedy construction. Moreover, after two barycentric subdivisions, for each PL maximum, the triangle spanned by the PL maximum, its neighbor vertex with highest value and their common neighbor with highest value is critical by the greedy construction (Figure 6). Finally, for each PL regular saddle, there is a critical edge spanning the PL saddle and its neighbor of lowest value in the component of the lower star not containing the absolute minimum.

(a) Regularity of the Greedy Construction

On a triangulated surface, two consecutive cells of a $\mathcal{V}$–path combinatorially differ by a single vertex (Figure 7). A $\mathcal{V}$–path $\blacktriangleleft\tau_0\ \sigma_0\ \tau_1 \dots \sigma_{k-1}\ \tau_k\blacktriangleright$ is said to be *decreasing* if the value of f on the first vertex (i.e. the vertex of $\sigma_0 \backslash \tau_1$) is greater than the value of f on the last vertex of the gradient step (i.e. the vertex of $\sigma_{k-1} \backslash \tau_{k-1}$). We first prove that, on triangulated surfaces, f is globally decreasing on each gradient path[2]:

Theorem 1. *Let $\mathcal{V}$ be the discrete gradient on triangulated surface K, obtained from the greedy construction ordered by scalar function f. Then the longest non-decreasing $\mathcal{V}$–path has length one, i.e. there is no two consecutive increasing steps.*

Proof. The proof of the theorem works equally with gradient path from vertex/edge or triangle/edge, and we detail here the triangle/edge case.

Consider a gradient $\mathcal{V}$–path $\blacktriangleleft\tau_0\ \sigma_0\ \tau_1\ \sigma_1\ \tau_2\blacktriangleright$, where τ_0, τ_1, τ_2 are edges and σ_0, σ_1 are adjacent triangles (Figure 7).

[1]The acyclicity test may use a union-find structure [42], leaving the bottleneck of the algorithm to the ordering of the pairs.

[2]Actually it is true for any dimension on *regular* $\mathcal{V}$–paths, i.e. $\blacktriangleleft\tau_0^{p\pm1}\ \sigma_0^p\ \tau_1^{p\pm1}\ \sigma_1^p \dots \sigma_{r-1}^p\ \tau_r^{p\pm1}\blacktriangleright$ with σ_i^p incident to at most 2 $(p\pm1)$–cells matched with a p–cell [26].

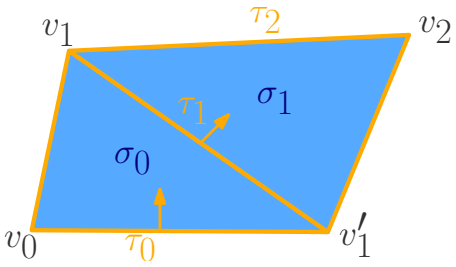

Figure 7: *Notation for the proof of Theorem 1.*

Denote by v_0 and v_1 the first and last vertices of $\blacktriangleleft\tau_0\ \sigma_0\ \tau_1\blacktriangleright$, v_1' and v_2 the first and last vertices of $\blacktriangleleft\tau_1\ \sigma_1\ \tau_2\blacktriangleright$.

We will prove that either $\blacktriangleleft\tau_0\ \sigma_0\ \tau_1\blacktriangleright$ is decreasing, or $\blacktriangleleft\tau_0\ \sigma_0\ \tau_1\ \sigma_1\ \tau_2\blacktriangleright$ are decreasing, i.e. either $f(v_0) > f(v_1)$, or $f(v_0) > f(v_2)$.

The greedy construction considered the pairs (τ_0, σ_0), (τ_1, σ_1), (τ_1, σ_0) and (τ_2, σ_1), ordered by their weights: $\mathsf{W}_f((\tau \prec \sigma)) = \bar{f}(\sigma) - \bar{f}(\tau)$ with:

$$\begin{aligned}
\bar{f}(\tau_0) &= \tfrac{1}{2}\left(f(v_0) + f(v_1')\right), \\
\bar{f}(\tau_1) &= \tfrac{1}{2}\left(f(v_1) + f(v_1')\right), \\
\bar{f}(\tau_2) &= \tfrac{1}{2}\left(f(v_1) + f(v_2)\right) \\
\bar{f}(\sigma_0) &= \tfrac{1}{3}\left(f(v_0) + f(v_1) + f(v_1')\right), \\
\bar{f}(\sigma_1) &= \tfrac{1}{3}\left(f(v_2) + f(v_1) + f(v_1')\right).
\end{aligned}$$

First, observe that pair (τ_1, σ_0) would not create a cycle when the two other pairs were considered: if pair (τ_1, σ_0) closed the cycle $\blacktriangleleft\tau_0'\ \sigma_0'\ \tau_1'\ \sigma_1'\ \dots \sigma_{k-1}'\ \tau_k'\blacktriangleright$ with $\tau_0' = \tau_k' = \tau_1$, $\sigma_0' = \sigma_0$ and thus $\sigma_{k-1}' = \sigma_1$, then pairs (τ_0, σ_0) and (τ_1, σ_1) would close the cycle $\blacktriangleleft\tau_1\ \sigma_1 = \sigma_{k-1}'\ \tau_{k-1}'\ \sigma_{k-2}'\ \dots \sigma_0' = \sigma_0\ \tau_0' = \tau_1\blacktriangleright$, but those pair were valid during the construction. Similarly, (τ_2, σ_1) would not create cycle at the time the other pairs were added, and was thus not considered first.
The proof boils down to two cases, depending on which pair was considered first:

case 1: pair (τ_0, σ_0) was considered before (τ_1, σ_1). According to the observation above, pair (τ_1, σ_0) has been considered after (τ_0, σ_0). Since the pairs are ordered by their weights, this implies that $\bar{f}(\sigma_0) - \bar{f}(\tau_1) > \bar{f}(\sigma_0) - \bar{f}(\tau_0)$, which gives $f(\tau_0) > f(\tau_1)$ and then $f(v_0) > f(v_1)$.

case 2: pair (τ_1, σ_1) was considered before (τ_0, σ_0). According to the same observation, pair (τ_1, σ_0) is considered after (τ_1, σ_1). Then $f(\sigma_0) - f(\tau_1) > f(\sigma_1) - f(\tau_1)$, so $f(\sigma_0) > f(\sigma_1)$, and thus $f(v_0) > f(v_2)$.

□

The corresponding work was published in Computer Aided Geometric Design, Elsevier, 2012..

(b) Minima Positioning

We now prove the relation between PL minima and the critical vertices given by the greedy construction. The result is valid under the assumption that f is "smooth" enough on the triangulated surfaces. The following theorem uses barycentric subdivision to supply to this smoothness requirement:

Theorem 2. *Let K' be the first barycentric subdivision of K, with scalar function f' linearly interpolated from f. Let $\mathcal{V}$ be the discrete gradient on K', obtained from the greedy construction ordered by f'. Then the PL minima as defined by Banchoff are critical vertices of $\mathcal{V}$.*

Proof. First note that the barycentric subdivision does not affect Banchoff's critical points, nor does it create any. In particular Banchoff's critical points always belong to K_0, and not to $K_0' \backslash K_0$.

Suppose, to obtain a contradiction, that v_m is a PL minimum but that it is not critical for $\mathcal{V}$ on K'. Then, there is an edge $e = (v_m v)$ matched with v_m. But v_m is a PL minimum, so $f(v_m) < f(v)$, and thus the pair (v_m, e) was considered after pair (v, e). Therefore, vertex v must have already been matched with another edge $e' = \{vw\}$. Since f' is linearly interpolated from f and vertex v is in-between v_m and w, we must have $f(v) < f(w)$. Then, $\blacktriangleleft v_m\ e\ v\ e'\ w \blacktriangleright$ would be an increasing gradient path of length greater than 1, leading to a contradiction with Theorem 1. □

(c) Maxima Positioning

In order to position correctly the minima, we needed to be sure that two minima are sufficiently far one from the other in the mesh. The case of maxima is similar, but we need a second barycentric subdivision, which is the same spacing between critical points as for the discrete Handlebody decomposition [38].

Theorem 3. *Let K'' be the second barycentric subdivision of K, with scalar function f obtained by linear interpolation. Let $\mathcal{V}$ be the discrete gradient on K'', obtained from the greedy construction ordered by f. Then for each PL maximum v, there is a critical triangle σ in the star of v. Moreover, σ is the triangle subdivided from vwx, where w is the adjacent vertex of v with the highest value and x is their common neighbor with the highest value (Figure 8).*

Proof. Let y be the other common neighbor of v and w. The ordering $f(v) > f(w) > f(x) > f(y)$ generates a partial ordering on the cells of the second barycentric subdivision, and subsequently another partially ordered set (poset) $\mathcal{P}$ on the pairs considered by the greedy strategy. The goal now is to prove that poset $\mathcal{P}$ guarantees that each pair involving σ is invalidated before it is considered. We follow the notation of Figure 8 for the vertices name, and denote each cell by the vertices it spans. The proof relies on analyzing poset $\mathcal{P}$, represented in Figure 9 and summarized in Figure 10. A poset arrow from one pair to another indicates that the first one is always considered before the second, for any values of f at v, w, x, y that satisfies $f(v) > f(w) > f(x) > f(y)$.

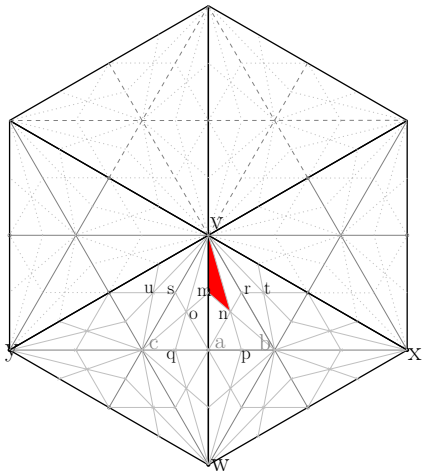

Figure 8: *Second barycentric subdivision around a maximum.*

For triangle mnv to be critical, it must not be matched with any of its three bounding edges: mv, mn or nv. First, we ensure that v is not matched with any of those edges. Indeed, pairs (v, sv), (v, tv) and (v, ov) are the roots of the poset, and thus if v is not matched outside the quadrilateral $vywx$, it would be first matched with either s, t, u or o.

Now, we check that each pair involving mnv is invalidated by another pair before it is considered.

$(mv \prec mnv)$: The pair $(mv \prec mnv)$ is invalidated by the matching of mv with mov, which is considered by the greedy construction first. The pair $(mv \prec mov)$ could have been prevented by matchings $(m \prec mv)$, $(v \prec mv)$, $(ov \prec mov)$ and $(mo \prec mov)$. The first two would also prevent the matching of mv with mnv, and the two last ones (actually all of them) are all considered after $(mv \prec mov)$. Therefore either $(m \prec mv)$, $(v \prec mv)$ or $(mv \prec mov)$ is added to $\mathcal{V}$ before, and thus prevent $(mv \prec mnv)$.

$(mn \prec mnv)$: The matching of mn with mnv is invalidated by the matching of mn with amn. The pair $(mn \prec amn)$ could be prevented by $(m \prec mn)$, $(n \prec mn)$, $(am \prec amn)$ and $(an \prec amn)$. The first two also prevent $(mn \prec mnv)$, and the last one is considered after $(mn \prec amn)$. Then, either $(mn \prec amn)$ is considered before $(am \prec amn)$, or $(am \prec amn)$ is invalidated either by $(m \prec am)$ or by $(am \prec amo)$. In that case, $(am \prec amo)$ is considered before $(ao \prec amo)$ and $(mo \prec amo)$. Therefore either $(m \prec mn)$, $(n \prec mn)$ or $(mn \prec amn)$ occur before and prevent $(mn \prec mnv)$.

$(nv \prec mnv)$: Last, the matching of nv with mnv is prevented by the matching of nv with nrv. This matching could be prevented by $(n \prec nv)$, $(v \prec nv)$, $(rv \prec nrv)$ or $(nr \prec nrv)$. The first two would also prevent

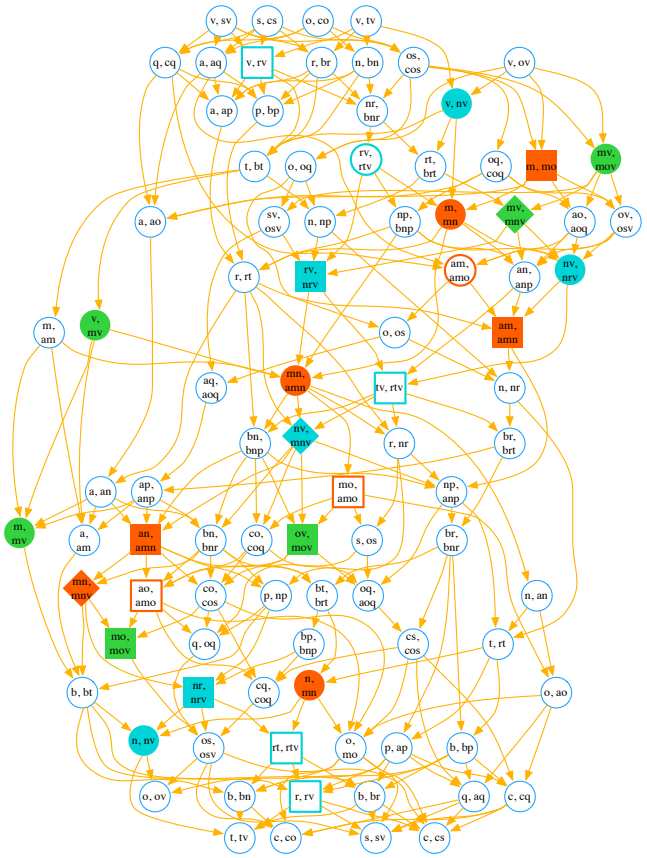

Figure 9: *Poset $\mathcal{P}$ generated by $f(v) > f(w) > f(x) > f(y)$ onto the pairs of incident cells: the matchings that would forbid mnv to be critical are marked by coloured diamonds, the one that would prevent these diamonds are marked as circles of the same colour, and the ones that would prevent the circles are marked with rectangles.*

$(nv \prec mnv)$, and the last one is considered after $(nv \prec nrv)$. Then, pair $(rv \prec nrv)$ is invalidated by $(rv \prec rtv)$, since the latter is considered before $(r \prec rv)$, $(rt \prec rtv)$ and $(tv \prec rtv)$ and we know that v does not match with rv.

All the possible matchings involving mnv are thus invalidated before they are considered in the greedy order derived from f. Therefore, mnv remains unmatched and is a critical triangle at the end of the greedy construction. □

(d) Saddle Positioning

The saddle case is very similar: PL saddle vertices generate critical edges in their star (Figure 11). The proof of the following follows the same lines as the maximum case, and is detailed in Lewiner's thesis [26].

Theorem 4. *Let K'' be the second barycentric subdivision of K, with scalar function f obtained by linear interpolation. Let $\mathcal{V}$ be the discrete gradient on K'', obtained by greedy construction from f. Then for each of Banchoff's saddle v, there is a critical edge in the star of v.*

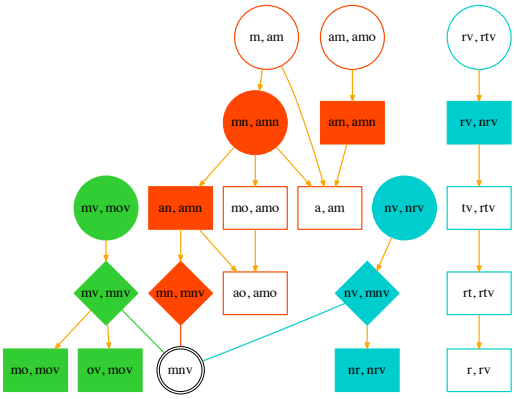

Figure 10: *Reduced version of the poset of Figure 9*

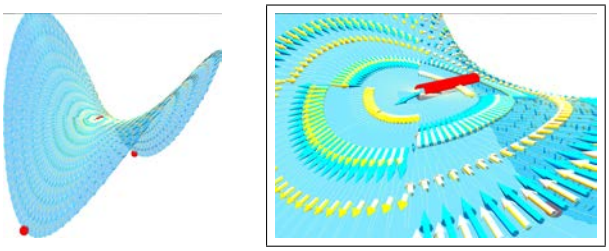

Figure 11: *The result of the greedy construction on a saddle with f being the vertical projection. The critical vertices are drawn as red balls, and the critical edge as a red cylinder. The vertex/edge pairs are draw with yellow arrows, while edge/triangle are drawn with blue arrows.*

(e) Limitations and Extensions

The above results are limited by the regularity restriction and the eventual extra critical cells generated by the greedy approach. In practice, we very rarely observe critical cells not adjacent to a PL critical point, and indeed the greedy approach has been successfully used to generate discrete Morse functions with as few critical cells as possible [23, 24].

Those results may be generalized to higher dimension. On the one hand, the dimension mainly increases the poset size but the analysis may be lead in a similar way. On the other hand, it would greatly contribute to discrete Morse theory applications since Banchoff's classification from the lower star gets much more intricate in higher dimension. The proofs may also be adapted to other constructions, in particular varying the weight definition and matching strategy [35].

4 Applications

Forman's discrete Morse theory is computationally efficient: the dominant execution time of the greedy construction is essentially the sorting of the pairs, which has asymptotic complexity $O(n \log n)$, where n is the number of cells multiplied by the average cell valence. It also gains robustness from avoiding numerical integration, and this guarantees the topological coherence of the result. This turns

Forman's definition more suitable for large-scale data analysis [8]. However, it lacked an intuitive connection with smooth Morse theory. The results of the previous section guarantee that the greedy construction correctly captures the features of f (at least in the PL sense), provided f is smooth enough. This allows building on the intuition of approximate critical points in applications using Forman's approach.

This opens the variety of applications of PL Morse theory [12, 3, 30, 17, 18] to Forman's case. We mention three of them, each one emphasizes a different aspect of this opening: the Morse-Smale decomposition, since the greedy algorithm is straightforward in any dimension, while PL approaches are delicate [12, 13] ; the persistence computation, for the similarity with its first computational formulation [9, 11]; and Reeb graphs since the algorithmic complexity is similar to the optimal ones [21, 4, 7, 34].

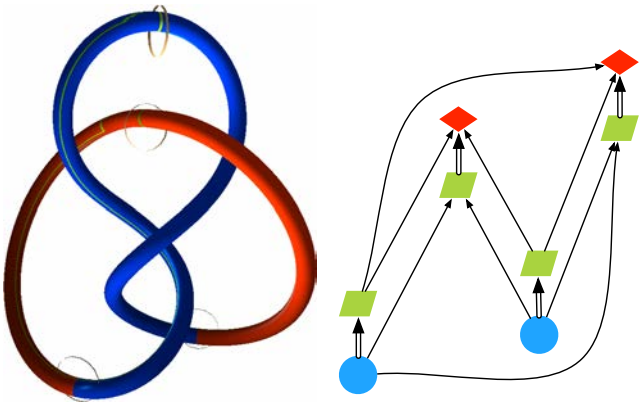

Figure 12: *Unstable basins on a knotted torus obtained from the greedy construction with f being the vertical projection. Saddles are outlined, together with their separatrixes (left) and the combinatorial structure of the $K_{\mathcal{M}}$: faces (maxima) are colored in red, edges (saddles) in green and vertices (minima) in blue (right).*

(a) Morse-Smale Decomposition

The Morse-Smale decomposition [40, 31] is a cell complex $K_{\mathcal{M}}$ built out of an original surface $\mathcal{M}$ with identical geometric realization, where each cell correspond to the largest set with similar dynamics under $-\nabla f$. It is constructed from the intersection of the stable and unstable basins of each critical point τ, where the stable basin is the union of all integral lines ending at τ and the unstable basin is the union of all integral lines starting near τ[3]. For computer applications, this Morse-Smale decomposition has been previously built in the PL setting using numerical integration [12, 13], and in the Forman setting by fixing first the critical points [25, 5, 26] or detecting them during the construction [18].

Once the gradient field has been constructed by the greedy strategy, the computation of this decomposition is straightforward. Since there is no closed $\mathcal{V}$–path, the set of $\mathcal{V}$–paths starting or ending at a critical cell is essentially a set of trees, which is traversed in linear time. During the traversal starting (resp. ending) at a critical cell τ, each cell of the path is marked by τ as origin (resp. destination). This gives the basin decomposition as defined by Forman [16]. However, vertices are never marked by a maximum, since maxima generate edge/triangle paths, and similarly triangles are never marked by a minimum. We can copy the mark of a triangle to its vertices and partition the set of vertices by grouping all vertices having the same start/end mark. Those basins can also be constructed from the critical edges, by looking in the path tree the $\mathcal{V}$–paths linking the saddle to minima and maxima. Those paths are the separatrices [43, 44] and the basins are obtained by a vertex conquer algorithm starting from those (Figure 12). The complexity of both constructions is linear in execution time and memory, once the discrete gradient has been computed, with simple algorithms [26].

[3] Indeed this is possible if adding a regularity condition on f, namely not having tangential integral lines at critical points.

(b) Persistence

Persistence is a widely used tool to filter out noise on the function f or on the sampling of K that generated spurious critical points. It has been used in Smale's proof of Poincaré's conjecture [40] and then introduced in a computational setting [11], with recent stability guarantees [6].

Persistence diagram took inspiration in the incremental algorithm to compute Betti numbers [9], where cells are successively added to the cell complex and can form cancellation pairs with previously inserted cells that increase or decrease certain Betti numbers, similarly to the greedy construction. The persistence diagram is then the graphs of each Betti number during the construction, when reducing to potential cancellation pairs of critical points.

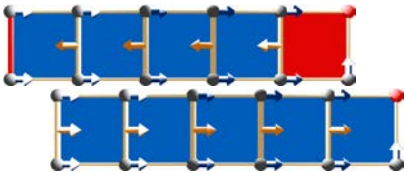

Figure 13: *Cancellation of the left critical edge with the right critical face (left) by inverting the unique $\mathcal{V}$–path between them (right).*

The greedy construction is similar in nature from this approach, and Forman's framework facilitates the reduction to critical pairs. The cancellation of a critical pair is performed by inverting a $\mathcal{V}$–path between the two critical cells (Figure 13). In order to maintain a valid discrete gradient, no closed path should be generated, and therefore it must be asserted that there is a unique $\mathcal{V}$–path between the critical cells. Contrarily to numerical integration, this test is extremely simple due to the graph structure of the set of all $\mathcal{V}$–paths, which is summarized by $K_{\mathcal{M}}$ (Figure 12). The structure is directly updated for subsequent cancellations. The complexity is similar to the PL case, where the dominant time is consumed by maintaining an ordered list of cancellation pairs.

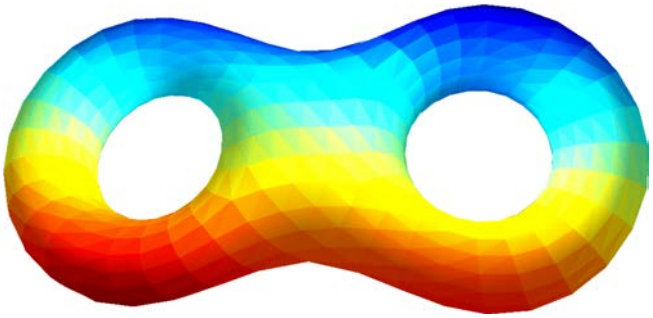

(a) Original complex with color coding of the geometric function.

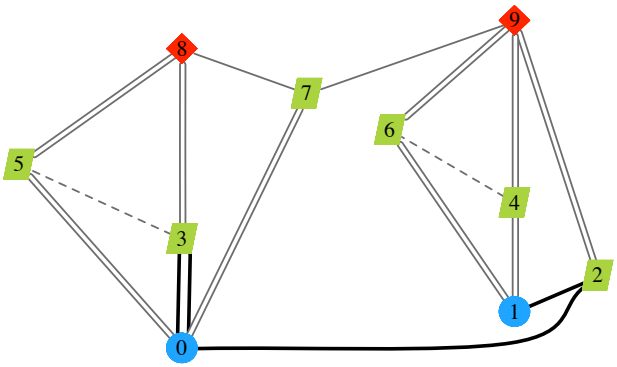

(b) The Morse–Smale diagram have two loops made of double edges (dotted lines).

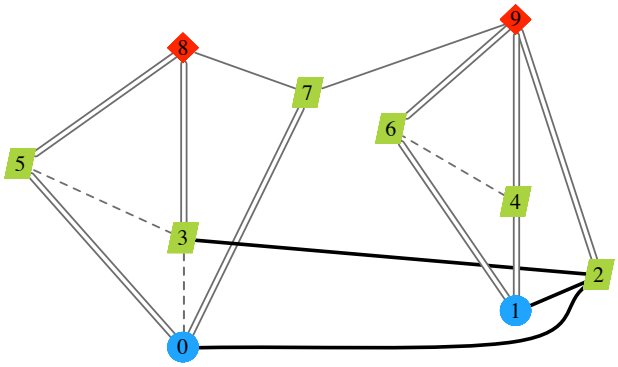

(c) First rotation: from $0 \to 3$ and $0 \to 2$, $0 \to 3$ is replaced by $2 \to 3$.

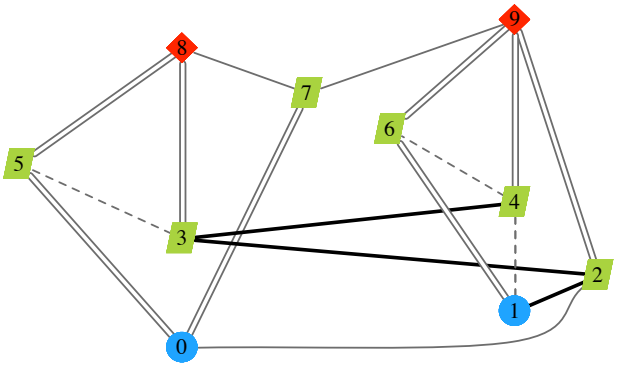

(d) Second rotation: from $1 \to 4$ and $1 \to 2 \to 3$, $1 \to 4$ is replaced by $3 \to 4$.

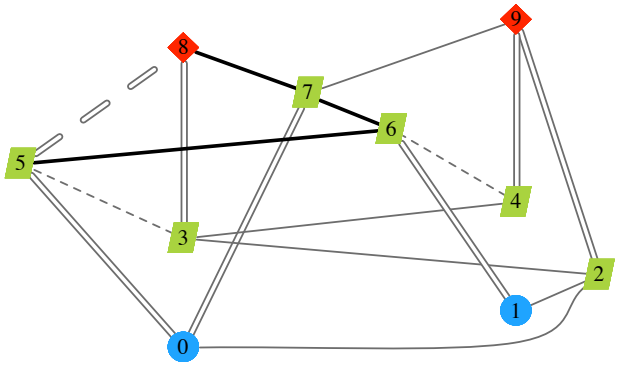

(e) Third rotation: from $9 \to 6$ and $9 \to 7$, $9 \to 6$ is replaced by $7 \to 6$. Fourth rotation: from $8 \to 5$ and $8 \to 7 \to 6$, $8 \to 5$ is replaced by $6 \to 5$.

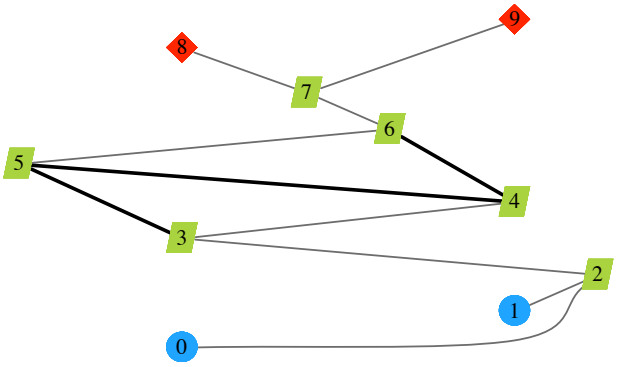

(f) Last reductions: $0 \to 5$, $0 \to 7 \to 6 \to 5$ and $0 \to 2 \to 3 \to 4$, $8 \to 7 \to 6 \to 5$ and $8 \to 3 \to 4$, $9 \to 4$ $9 \to 2 \to 3 \to 4$ and $9 \to 7 \to 6 \to 5$, and $0 \to 5$ and $0 \to 2 \to 3 \to 4$ all lead to $4 \to 5$. Finally, $1 \to 6$ and $1 \to 2 \to 3 \to 4$ lead to $4 \to 6$.

Figure 14: *Transforming a Morse–Smale decomposition in Reeb graph.*

The corresponding work was published in Computer Aided Geometric Design, Elsevier, 2012..

(c) Reeb Graphs

Reeb graphs and contour trees have received a lot of attention from the visualization community [14, 32], where it is used to resume the behavior of a scalar function, typically to guess the topology of its isosurfaces [20, 45]. Reeb graphs are obtained by identifying two points with the same image f_0 through f and lying in the same connected component of $f^{-1}(\mathsf{f}_0)$. It is interpreted as a graph with nodes at bifurcations, which are exactly the critical points according to Morse lemma.

The main observation here is that Reeb graphs are essentially a reduction of Morse-Smale diagrams: in the latter, saddles are connected to the minima and maxima of the adjacent basins, while in Reeb graphs saddles with one common minimum or maximum are directly connected, according to their values through f. More precisely, consider two saddles s_1 and s_2, $f(s_1) < f(s_2)$, incident in the Morse diagram to minima v_1 and v_2 for s_1, and v_2 and v_3 for s_2. The Reeb graph only represent the incidence of s_2 onto s_1 and v_3, and does not detail whether s_2 is also incident to v_1 or v_2.

We obtain the Reeb graph by successive rotation in the graph that replace links similar to s_2v_2 for s_2s_1, similarly to contour tree approaches [21] (Figure 14). Only loop connection between saddles [7] (dotted lines in Figure 14(b)), which mark the presence of two $\mathcal{V}$–paths between critical points, generate multiple rotations (Figure 14(f)). The complexity of the whole algorithm is dominated by the construction of $\mathcal{V}$, which is $O(n \log n)$, similarly to other optimal techniques [4, 34].

5 Conclusions and Future Work

In this work, we proved that, under mild regularity conditions, the greedy construction of discrete vector fields actually captures the critical features in the piecewise-linear sense. We point out several applications that could gain from the robustness of Forman's setting without loosing the intuition behind critical points thanks to our theoretical results.

The approach used here can be extended in two directions. First, by constructing similar posets for three–dimensional meshes, those guarantees may be extended to volumetric meshes, where the greedy approach is significantly simpler than PL constructions [13]. Second, other approaches have been devised to construct discrete gradient fields, in particular using geometric weights or other matching strategies [35]. The analysis may be more complex, since it would depend on the shape of the triangles, but with the sophistication of Reininghaus' algorithms should help in obtaining sharper guarantees.

Acknowledgements The author would like to thank Profs. Jean-Daniel Boissonnat and Hélio Lopes for supervising his Ph.D.'s, and Profs. Günter Ziegler and Konrad Polthier for their post-doc supervision and assistance during the preparation of this work. This work is partially financed by EDX, MATHEON, CNPq, INRIA and FAPERJ.

References

[1] E. Babson and P. Hersh. Discrete Morse functions from lexicographic orders. *Transactions of the American Mathematical Society*, 357:509–534, 2005.

[2] T. Banchoff. Critical points and curvature for embedded polyhedra. *Journal of Differential Geometry*, 1:257–268, 1967.

[3] P. Bremer, B. Hamann, H. Edelsbrunner and V. Pascucci. A topological hierarchy for functions on triangulated surfaces. *Transactions on Visualization and Computer Graphics*, 10(4):385–396, 2004.

[4] H. Carr, J. Snoeyink and U. Axen. Computing contour trees in all dimensions. *Computational Geometry: Theory and Applications*, 24:75–94, 2000.

[5] F. Cazals, F. Chazal and T. Lewiner. Molecular shape analysis based upon Morse–Smale complex and the Connolly function. In *Symposium on Computational Geometry*, pages 351–360. ACM, 2003.

[6] D. Cohen–Steiner, H. Edelsbrunner and J. L. Harer. Stability of Persistence Diagrams. In *Symposium on Computational Geometry*, pages 263–271. ACM, 2005.

[7] K. Cole–McLaughlin, H. Edelsbrunner, J. L. Harer, V. Natarajan and V. Pascucci. Loops in reeb graphs of 2-manifolds. In *Symposium on Computational Geometry*, pages 344–350. ACM, 2003.

[8] M. Day, J. Bell, P. Bremer, V. Pascucci, V. Beckner and M. Lijewski. Turbulence effects on cellular burning structures in lean premixed hydrogen flames. *Combustion and Flame*, 156(5):1035–1045, 2009.

[9] C. J. A. Delfinado and H. Edelsbrunner. An incremental algorithm for Betti numbers of simplicial complexes. In *Symposium on Computational Geometry*, pages 232–239. ACM, 1993.

[10] S. Dong, P. Bremer, M. Garland, V. Pascucci and J. Hart. Spectral surface quadrangulation. *Transactions on Graphics*, 25(3):1057–1066, 2006.

[11] H. Edelsbrunner, D. Letscher and A. Zomorodian. Topological persistence and simplification. In *Symposium on Foundations of Computer Science*, pages 454–463, 2000.

[12] H. Edelsbrunner, J. L. Harer and A. Zomorodian. Hierarchical Morse complexes for piecewise linear 2–manifolds. In *Symposium on Computational Geometry*, pages 70–79. ACM, 2001.

[13] H. Edelsbrunner, J. L. Harer, V. Natarajan and V. Pascucci. Morse–Smale complexes for piecewise linear 3–manifolds. In *Symposium on Computational Geometry*, pages 361–370. ACM, 2003.

[14] A. Fomenko and T. Kunii. *Topological modeling for visualization*. Springer, 1997.

[15] R. Forman. A discrete Morse theory for cell complexes. In S. T. Yau, editor, *Geometry, Topology and Physics for Raoul Bott*, pages 112–115. International Press, Cambridge, 1995.

[16] R. Forman. Discrete morse theory and the cohomology ring. *Transactions of the American Mathematical Society*, 354:5063–5085, 2002.

[17] A. G. Gyulassy, V. Natarajan, V. Pascucci and B. Hamann. Efficient computation of morse-smale complexes for three-dimensional scalar functions. *Transactions on Visualization and Computer Graphics*, 13(6):1440–1447, 2007.

[18] A. G. Gyulassy, P.-T. Bremer, B. Hamann and V. Pascucci. A practical approach to morse-smale complex computation: Scalability and generality. *Transactions on Visualization and Computer Graphics*, 14(6):1619–1626, 2008.

[19] M. Joswig and M. Pfetsch. Computing optimal discrete Morse functions. *Electronic Notes in Discrete Mathematics*, 17:191–195, 2005.

[20] M. Van Kreveld, R. Van Oostrum, C. Bajaj, V. Pascucci and D. Schikore. Contour trees and small seed sets for isosurface traversal. In *Symposium on Computational Geometry*, page 220. ACM, 1997.

[21] F. Lazarus and A. Verroust. Level Set Diagrams of Polyhedral Objects. In *Solid Modeling and Applications*, pages 130–140. ACM, 1999.

[22] T. Lewiner. Constructing discrete Morse functions. Master's thesis, *Department of Mathematics, PUC–Rio*, Aug. 2002. Advised by Hélio Lopes and Geovan Tavares.

[23] T. Lewiner, H. Lopes and G. Tavares. Optimal discrete Morse functions for 2–manifolds. *Computational Geometry: Theory and Applications*, 26(3):221–233, 2003.

[24] T. Lewiner, H. Lopes and G. Tavares. Towards optimality in discrete Morse theory. *Experimental Mathematics*, 12(3):271–285, 2003.

[25] T. Lewiner, H. Lopes and G. Tavares. Applications of Forman's discrete Morse theory to topology visualization and mesh compression. *Transactions on Visualization and Computer Graphics*, 10(5):499–508, 2004.

[26] T. Lewiner. Geometric discrete Morse complexes. PhD thesis, *Department of Mathematics, PUC–Rio*, Aug. 2005. Advised by Hélio Lopes and Geovan Tavares.

[27] T. Lewiner, H. Lopes, E. Medeiros, G. Tavares and L. Velho. Topological mesh operators. *Computer Aided Geometric Design*, 27(1):1–22, 2010.

[28] J. W. Milnor. *Morse theory*. Number 51 in *Annals of Mathematics Study*. Princeton University Press, 1963.

[29] M. Morse. Relations between the critical points of a real function of n independent variables. *Transactions of the American Mathematical Society*, 27:345–396, 1925.

[30] V. Natarajan and V. Pascucci. Volumetric data analysis using Morse-Smale complexes. In *Shape Modeling and Applications*, pages 320–325. IEEE, 2005.

[31] J. Palis and W. de Melo. *Geometric theory of dynamical systems: an introduction*. Springer, New York, 1982.

[32] V. Pascucci, G. Scorzelli, P. Bremer and A. Mascarenhas. Robust on-line computation of Reeb graphs: simplicity and speed. In *Siggraph*, page 58. ACM, 2007.

[33] V. Pascucci, X. Tricoche, H. Hagen and J. Tierny, editors. *Topological Methods in Data Analysis and Visualization*. Springer, 2011.

[34] G. Patanè, M. Spagnuolo and B. Falcidieno. A minimal contouring approach to the computation of the Reeb graph. *Transactions on Visualization and Computer Graphics*, pages 583–595, 2009.

[35] J. Reininghaus and I. Hotz. Combinatorial 2d vector field topology extraction and simplification. In *TopoInVis*, pages 103–114, 2009.

[36] J. Reininghaus, D. Günther, I. Hotz, S. Prohaska and H. Hege. TADD: A computational framework for data analysis using discrete Morse theory. In *Mathematical Software*, pages 198–208, 2010.

[37] J. Reininghaus, C. Löwen and I. Hotz. Fast combinatorial vector field topology. *Transactions on Visualization and Computer Graphics*, 17(10):1433–1443, 2011.

[38] C. P. Rourke and B. J. Sanderson. *Introduction to piecewise–linear topology*. Springer, New York, 1972.

[39] A. Sharf, T. Lewiner, G. Shklarski, S. Toledo and D. Cohen-Or. Interactive topology-aware surface reconstruction. In *Siggraph*, volume 26, pages 43.1–43.9, 2007.

[40] S. Smale. On dynamical systems. *Boletín de la Sociedad Matemática Mexicana*, 5(2):195–198, 1960.

[41] B. Stander and J. Hart. Guaranteeing the topology of an implicit surface polygonization for interactive modeling. In *Siggraph course notes*, page 44, 2005.

[42] R. E. Tarjan. Efficiency of a good but not linear set union algorithm. *Journal of the ACM*, 22(2):215–225, 1975.

[43] T. Weinkauf and D. Günther. Separatrix persistence: Extraction of salient edges on surfaces using topological methods. *Computer Graphics Forum*, 28(5):1519–1528, 2009.

[44] T. Weinkauf, Y. Gingold and O. Sorkine. Topology-based smoothing of 2d scalar fields with C1-continuity. *Computer Graphics Forum*, 29(3):1221–1230, 2010.

[45] Z. Wood, H. Hoppe, M. Desbrun and P. Schröder. Removing excess topology from isosurfaces. *Transactions on Graphics*, 23(2):190–208, 2004.

The corresponding work was published in Computer Aided Geometric Design, Elsevier, 2012..